NJC

Accepted Manuscript

ROYAL SOCIETY OF CHEMISTRY

rsc.li/njc

Supramolecular tripodal Au(I) assemblies in water. Interactions with pyrene fluorescent probe.

Andrea Pinto,[a,b] Guillem Hernández,[a] Raquel Gavara,[a] Elisabet Aguiló,[a] Artur J. Moro,[c] Gabriel Aullón,[a] Marc Malfois,[d] João Carlos Lima,[c] Laura Rodríguez.[a,b,*]

[a] *Departament de Química Inorgànica i Orgànica. Secció de Química Inorgànica. Universitat de Barcelona, Martí i Franquès 1-11, 08028 Barcelona, Spain. Tel.: +34 934039130. e-mail: laura.rodriguez@qi.ub.es*

[b] *Institut de Nanociència i Nanotecnologia (IN2UB). Universitat de Barcelona, 08028 Barcelona (Spain)*

[c] *LAQV-REQUIMTE, Departamento de Química, Universidade Nova de Lisboa, Monte de Caparica, Portugal.*

[d] *ALBA Synchrotron Light Laboratory (CELLS), Carrer de la Llum 2−26, 08290 Cerdanyola del Vallès, Barcelona, Spain*

Dedicated to Prof. Ernesto Carmona on occasion of his 70th anniversary.

View Article Online
DOI: 10.1039/C9NJ00469F

Abstract

The synthesis of three gold(I) tripodal complexes derived from tripropargylamine and containing the water soluble phosphines PTA (1, 3,5-triaza-7-phosphaadamantane), DAPTA (3,7-diacetyl-1,3,7-triaza-5-phosphabicyclo[3.3.1]nonane) and TPPTS (triphenylphosfine-3,3',3''-trisulfonic acid trisodium salt) is here described. The three complexes are observed to give rise to the formation of supramolecular aggregates in water and very long fibers. This property has been analyzed by means of ^{1}H-NMR spectroscopy at different concentrations and SAXS. The results point out the important role of the phosphine moieties as the main enthalpic or entropic contribution in the resulting Gibbs energy of aggregates formation.

The tripodal structure of the three complexes together with the presence of gold(I) atoms make them ideal candidates to interact with hydrophobic molecules also in water. For this, the interaction with pyrene in this solvent has been evaluated with successful results in all three complexes. The highest association constant corresponds to **2** as the host. DFT studies indicates the location of pyrene in the tripodal cavity as the most stable conformation. The interaction with pyrene has been additionally studied within cholate hydrogel matrixes pointing out the stability of the resulting host:guest adducts in the different medium.

Keywords: gold(I), tripodal, hydrogels, luminescence, pyrene

Introduction

Nature, especially in biological systems, has an extraordinary ability to develop complex and functional molecular assemblies employing reversible non-covalent interactions.[1] These examples from Nature have inspired chemists over the past several years to develop synthetic protocols to obtain complex assemblies employing supramolecular interactions such as hydrophobic forces, hydrogen-bonding, transition metal coordination, and gels formation among others.[2-6] These structures are worthy candidates to be involved in processes such as catalysis,[7-9] sensing,[10-13] artificial photo-capturing systems[14] or encapsulation among others.[15] Container (encapsulating) architectures can encage guest molecules within a confined space, dynamically harnessing multiple non-covalent interactions. In particular, encapsulation of planar hydrophobic molecules is an important strategy to remove from water pollutants with mutagenic and/or carcinogenic effects.[16,17] However, up to date the number of precedent examples of supramolecular metallocapsules that exhibit sufficient structural flexibility to adapt diverse substrates by adjusting the cavity size are scarce.[18-21,] The majority of examples are pure organic macrocyclic compounds such as calix[n]arenes, cyclodextrins, cucurbit[6]urils which can be water soluble and possess a hydrophobic cavity compared to water.[22-25] Less examples are described with metallocavitands acting as hosts.[26,27]

Furthermore, to the best of our knowledge, there are not found in the literature reports based on gold(I) systems as hosts for the molecular recognition of arenes in water, These kind of structures present the advantage of having additional points of interactions (*e.g.* Au···π, C-H···Au, N-H···Au)[28,29] that can improve their sensing process. Additionally, they can be designed to be obtained in short synthetic routes (1-2 steps) with moderate-high yields. An interesting way to proceed is based on the synthesis of tripodal gold(I) structures able to detect guest molecules within their open cavities. Although some investigations have been done regarding this for the recognition of cations in organic solvents,[30,31] as far as we know, there are not reports for the recognition of aromatic molecules in water. Taking into consideration all of this, we present herein the synthesis and characterization of three tripodal gold(I) complexes that are observed to self-assemble in aqueous medium giving rise to the formation of aggregates and very long fibers. The supramolecular structures contain hydrophobic

View Article Online
DOI: 10.1039/C9NJ00469F

(gold atoms atoms and alkynyl groups) and hydrophilic moieties (located at the phosphines). Previous work reported by us has been mainly based on linear mononuclear compounds containing aromatic chromophores that can improve the self-assembly process by the presence of $\pi - \pi$ interactions.[3,5,11,12,29] In this work, we can demonstrate that the absence of this type of interactions, based on the presence of aromatic chromophores, does not prevent intermolecular contacts and aggregation leading to the formation of very long fibers. The simplicity of the present molecules are particularly important since it can be demonstrated that only Au(I) and probably some hydrogen bonds coming from phosphine units are necessary in these supramolecular assemblies.

The ability of these large supramolecular hydrophobic aggregates to act as binding sites is successfully proved using pyrene as probe in aqueous medium. The choice of pyrene is based on its efficient fluorescence which has proved to be a useful tool for measuring hydrophobic environments as well as complex formation in host:guest processes.[23, 32-35]

The resulting weak host:guest interactions have been also tested in metal cholate hydrogels in order to compare their stability and to analyse the role gold(I) within this organic matrix.[36,37] Although a variety of metal cholates were shown to form hydrogels, to the best of our knowledge there are not examples of organometallic complexes included within this supramolecular hydrogelator structure.

View Article Online
DOI: 10.1039/C9NJ00469F

Results and Discussion

Synthesis and Characterization

The trinuclear phosphine Au(I) acetylides **1-3** were prepared by slight modifications on a previously reported method,[38] by treatment of [AuCl(PR_3)] (PR_3 corresponding to the water-soluble phosphines PTA, DAPTA and TPPTS) with terminal tripropargylamine in the presence of KOH base in methanol (Scheme 1). The three different phosphines (two neutral and one anionic) were carefully chosen due to the increasing degree of solubility in water (PTA < DAPTA < TPTTS) in order to study the potential correlation between the global solubility of the complexes in water and the observed aggregation motifs.

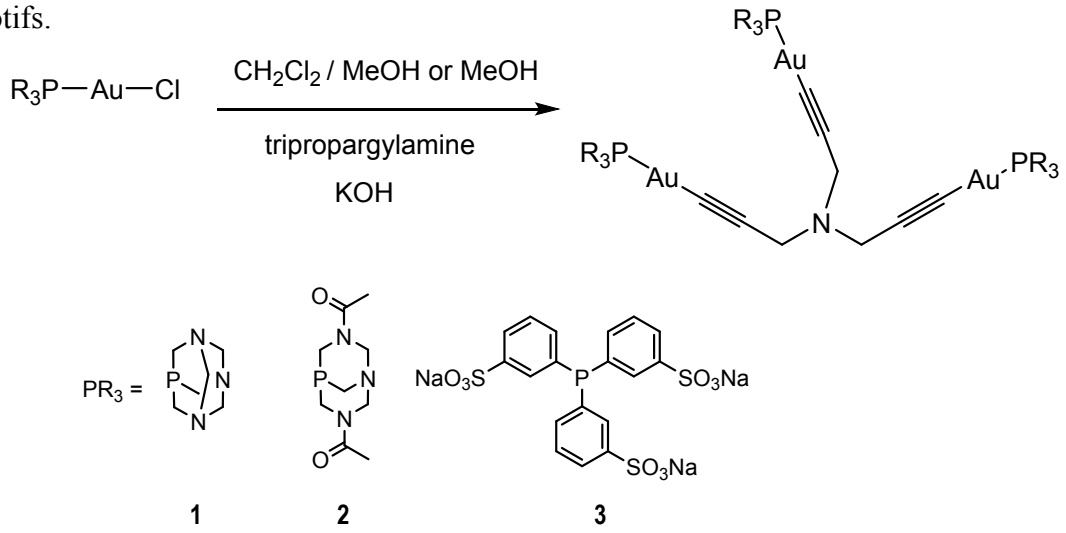

Scheme 1. Synthesis of complexes **1-3**.

The reaction was performed in CH_2Cl_2/MeOH (in the case of **1** and **2**) or MeOH (in the case of **3** in order to improve the solubility of the AuCl(PR_3) reactant) and the solution reaction was protected from light with aluminum foil and stirred at room temperature for *ca*. 3h. The resulting compounds were obtained in pure form after filtration through Celite and recrystallization with dichloromethane/hexane.

^{31}P NMR spectra display single resonances at -40.1 ppm (**1**), -13.9 (**2**) and 42.5 ppm (**3**) in accordance with P-donor coordination to the metal center. ^{1}H NMR shows the disappearance of the signal related to the tripropargylamine terminal proton at *ca.* 2.3

ppm, as the main indication of the successful formation of the products. Additionally, the methylene proton of the N-CH_2-C≡C moiety (*ca.* 3.50 ppm) appears as a singlet instead of the doublet observed in the propargylamine starting material, due to the coupling with the terminal alkynyl proton (Figures 1 and S1-S5). This methylene proton becomes much broader and almost disappear in the case of **1** (containing the less soluble phosphine) in D_2O (see Figure S6), being an indicative of the formation of supramolecular aggregates in this solvent (see Aggregation behaviour Section).

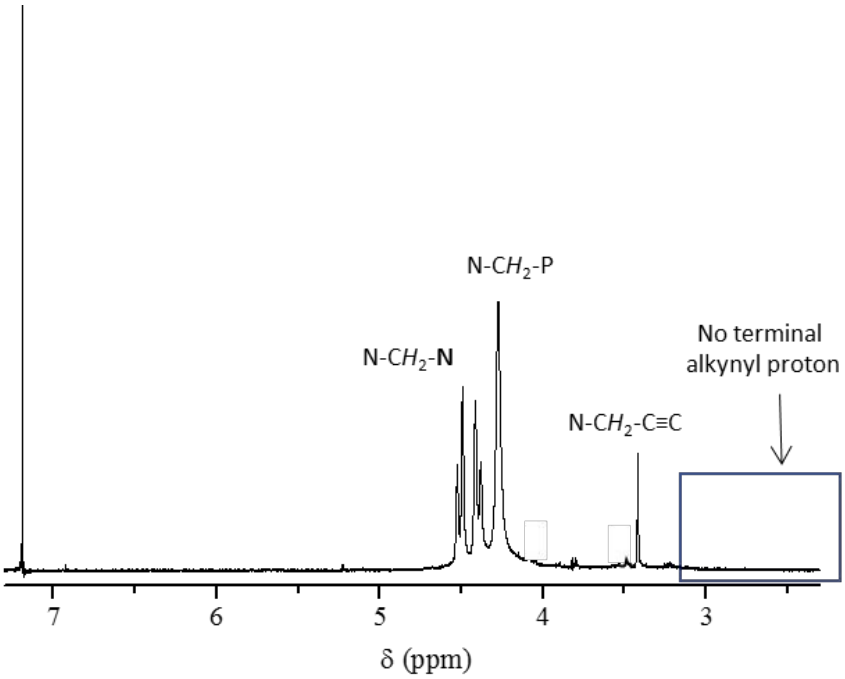

Figure 1. ^{1}H-NMR spectrum of **1** in $CDCl_3$.

Infrared spectra show additional evidence of the successful formation of the products due to the disappearance of the signal related to the terminal alkynyl at 3100-3000 cm^{-1} in the final products. Mass spectra confirmed in all cases the correct formation of the products with the corresponding m/z [M+H$^+$] peaks detection in **1** and **2** and [M- 7 Na$^+$+ 4H$^+$ + 3 H_2O]$^{3-}$ in **3**.

Aggregation behaviour

^{1}H-NMR data recorded at different concentrations and times are a direct evidence of the formation of aggregates. There is a linear correlation between the area of the phosphine protons and concentration in fresh solutions (Figures S7-8). Additionally, as observed in

Figure 2, there is a slight upfield shift of the N-CH_2-N phosphine protons at *ca.* 4.8 ppm (red arrow) upon aggregation with time, being a direct indication of the involvement of this unit in the formation of the supramolecular structures. This shift is accompanied with a decrease on the phosphine protons integration with time, due to the expected broadening of the aggregated protons, and the observation of precipitate formation in the solution.

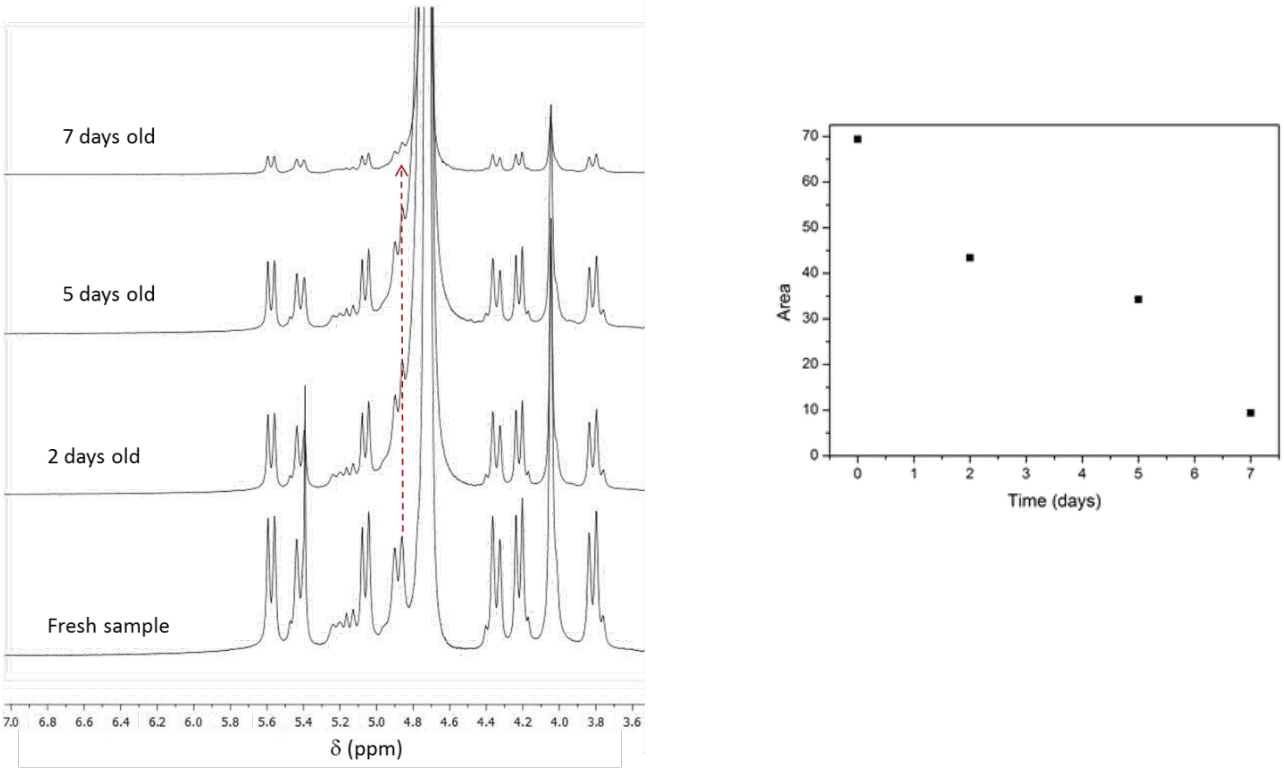

Figure 2. ^{1}H NMR spectra of **2** at 2.6·10^{-3}M concentration in D_2O recorded in freshly prepared solutions and after 2, 5 and 7 days (left); Variation on the area of the more downfield shifted phosphine proton upon aggregation with time (right).

The size and shape of the aggregates were measured by SAXS at different concentrations (1·10^{-4} M, 5·10^{-5} M, 1·10^{-5} M and 5·10^{-6} M) in water, at different temperatures (from 20 ºC to 40 ºC in a 5 ºC gradient) and one week after their preparation in order to favor aggregation. The low-resolution structures were reconstructed ab initio from the scattering patterns using the DAMMIN program[39] (see some examples in Figures 3 and S9-11). Smaller size aggregates were recorded at higher concentrations, mainly in the case of the more water soluble complexes **2** and **3**.

This can be due to the precipitation of the complexes in the medium when increasing concentration, giving rise to larger structures unable to be detected by SAXS. This is in agreement with the observed fibers' formation (see below optical microscopy characterization) and the aggregation detected by NMR for one-week-old solutions (Figure 2). This behavior was already observed recently for other gold(I) complexes that aggregate in water.[12] Higher concentrations, in the order of *ca*. 10^{-3} M as those used for NMR experiments, were not possible to be measured by SAXS precluding a strict comparison between these two techniques.

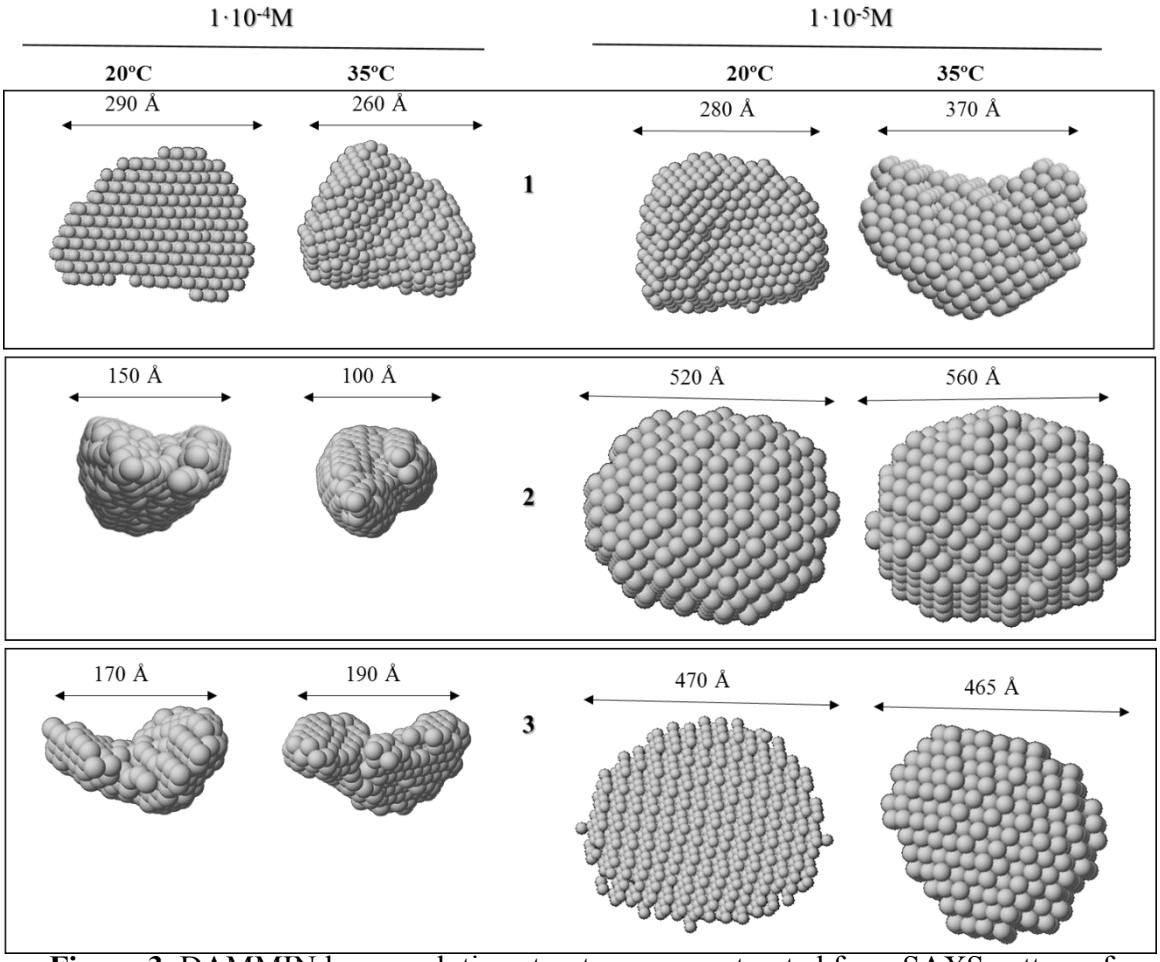

Figure 3. DAMMIN low-resolution structures reconstructed from SAXS patterns for $1\cdot10^{-4}$ M (left) and $1\cdot10^{-5}$ M (right) solutions of **1** (top), **2** (middle) and **3** (bottom) in water.

In general, temperature does not affect substantially the aggregates' size. Nevertheless, in some cases (compound **1** at $1\cdot10^{-5}$ M and compounds **2** and **3** at $5\cdot10^{-5}$ M concentrations) there is a variation around 100 Å (large enough to discard as error

deviation). While an increase on the size is measured in complex **1** (280 Å at 20ºC and 370 Å at 35 ºC), a decrease can be detected for **2** and **3** (340-300 Å at 20ºC and 230-200 Å at 35 ºC). This may be attributed to a more hydrophobic character of **1**, being hydrophobic interactions more favored at higher temperatures. In the case of **2** and **3**, it is expected that hydrogen bonding intermolecular contacts, due to the presence of oxygen atoms in their phosphine ligands, are disfavored at higher temperatures,[40] giving rise to smaller structures. Similar behavior was previously detected by us with PTA and DAPTA gold(I) derivatives where the entropic factor (due to the release of water molecules upon aggregation) was the driving force for the aggregates' formation in the first case (PTA, and in our case complex **1**). This was the most important contribution on the calculated negative Gibbs energy for the aggregation process. On the contrary, enthalpic factors become more important for DAPTA complex **2** (and extensively for complex **3**) where additional hydrogen bonding contacts may be established between the oxygen atoms of the phosphine and the solvent.[41]

Optical microscopy images show that the resulting translucent empty fibers can grow up to hundreds of micrometers length and *ca*. 5 micrometers width (Figure 4). At lower concentrations the fibers are thinner and cleaner as depicted in Figures 4 and S12, building up to the formation of well-defined fibrillary self-assembled structures.

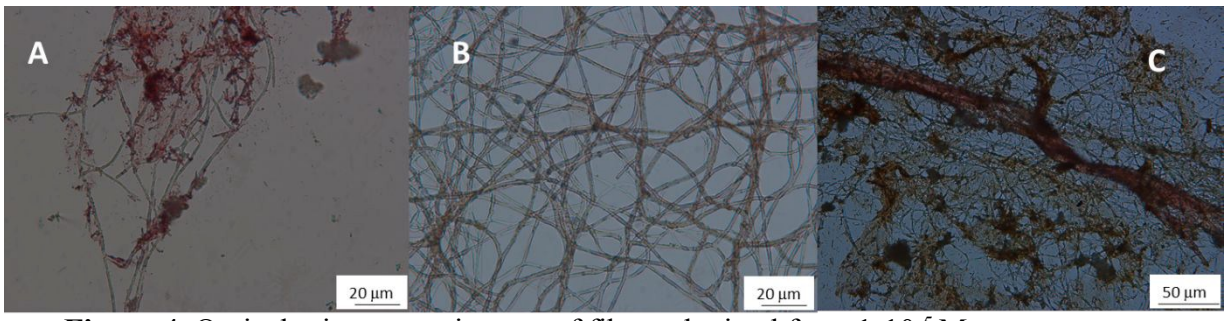

Figure 4. Optical microscopy images of fibers obtained from $1 \cdot 10^{-5}$ M aqueous solutions of **1** (A), **2** (B) and **3** (C). 100x magnification.

Supramolecular interactions with pyrene

The tripodal nature and the presence of gold(I) atoms in compounds **1-3** make them ideal candidates to be used as hosts by using the hydrophobic counterparts for the interaction with aromatic (and hydrophobic) guests in water.

Absorption differential spectra of $1 \cdot 10^{-5}$ M solution of pyrene in the presence of increasing amounts of host display no significant variations. It is worth to mention an increase on the light dispersion probably due to the presence of host aggregates in water that can interact with pyrene molecules (see below emission titrations). This dispersion of light is less observed in the presence of complex **3** due to its better solubility in water (Figures S13-15). The calculated pyrene solubility in water based on absorption spectra (Figures S13-15) and its reported molar absorption coefficient at 336 nm (32.500 $M^{-1} \cdot cm^{-1}$, [42]) is 0.77 μm, which is in agreement with the literature. [43] This means that this is the only amount of pyrene solubilized in water from the $1 \cdot 10^{-5}$ M solution prepared. The rest, is expected to be involved in the interaction process with gold(I) tripodal complexes giving rise to larger adducts that are affecting the dispersion baseline. In this way, free pyrene is removed from aqueous solution due to its solubilization by its interaction with the hydrophobic gold(I) host systems, giving rise to the formation of small aggregates that may present a very small absorptivity coefficient as indicated by the small increase of the absorption upon complex formation.

Emission titration data display a decrease on the pyrene intensity in the presence of the tripodal complexes (Figures S16-18). The recorded fluorescence quenching of pyrene observed from the interaction with gold(I) receptors follows the same behaviour previously shown in other supramolecular systems containing hydrophobic inner cavities such as by calix[4]arene and calix[4]resorcinarenes.[44] Thus, it should be expected a partially supramolecular host···guest adduct formation between the pyrene and the gold(I) structures giving rise to the formation of non-emissive Au···π and/or C-H···π assemblies,[45] present in very small dispersive state in solution (according to absorption scattering) that are also quenching the emission of the free pyrene solubilized in water. The recorded decrease on intensity follows the trend **2** > **3** > **1**, as an indication of the expected more efficient host:guest contact in the presence of better water soluble gold(I) hosts **2** and **3**. Additionally, the plot of the intensity at the emission maxima versus concentration indicates a change on the slope at one equivalent of gold(I) complex, in agreement with 1:1 interaction.

Similar titrations carried out in the absence of oxygen do not display the presence of pyrene phosphorescence as a consequence of a triplet population by intersystem crossing due to heavy atom effect.[46] Additionally, the band at 473 nm corresponding to

the pyrene excimer formation is not observed in the fluorescence emission spectra neither in the presence nor in the absence of the receptor.

^{31}P NMR titrations of gold complexes in the presence of 0.5, 1 and 2 equivalents of pyrene display a *ca*. 0.5 ppm upfield shift of the phosphorous signal upon interaction with the aromatic molecule and this shift is maintained constant from 1 equivalent, supporting the 1:1 complex formation (Figure 5). This means that pyrene molecule is clearly affecting the chemical vicinity of the phosphine, although no direct coordination is expected due to the small chemical shift variations. The first and larger effect observed in the presence of 0.5 equivalents of pyrene indicates the formation of a quite stable intermediate corresponding to the 2:1 (gold complex: pyrene) adduct which could be detected by mass spectrometry with the corresponding M + H^+- 4 Au-DAPTA + CH_2Cl_2 + 5 H_2O peak at *m/z* 1490.1.2 (being M = 2 * (**2**) + pyrene). The formation of this type of pyrene 2:1 adducts was previously observed with organic capsules.[47]

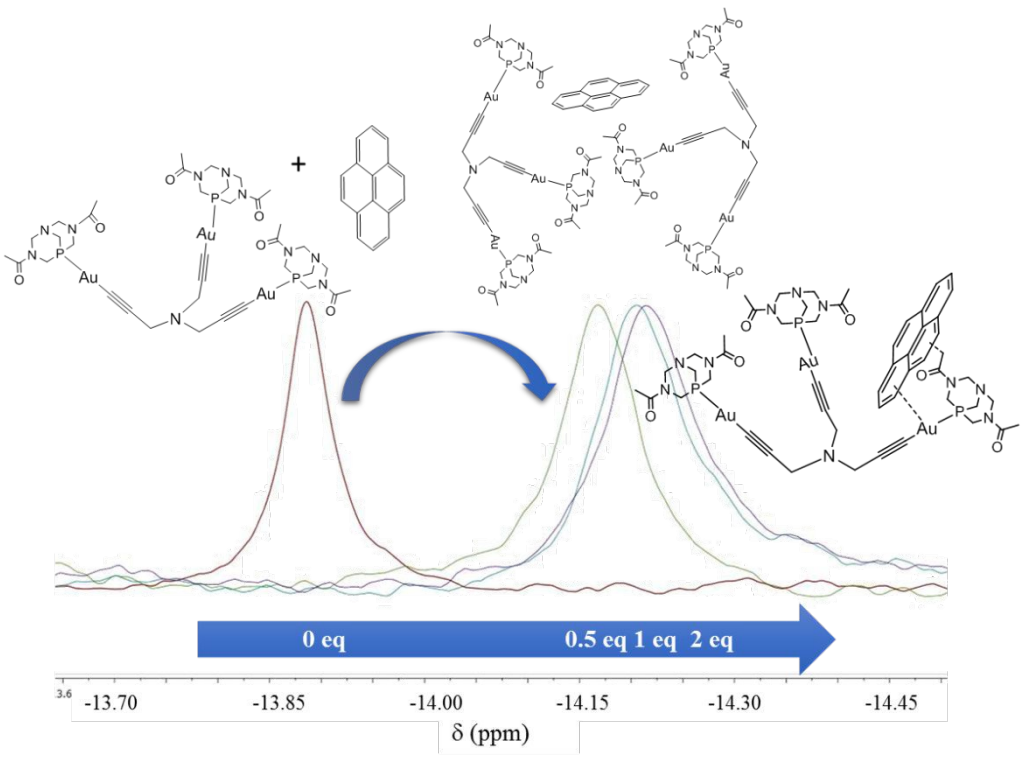

Figure 5. ^{31}P{^{1}H} NMR spectra of **2** in D_2O in the absence (left) and in the presence of increasing amounts of pyrene dissolved in CD_3OD.

The size of the resulting host:guest supramolecular assemblies depends on the solubility in water of the complexes as evidenced by SAXS. Thus, the resulting 1:1 adduct from $1 \cdot 10^{-5}$ M aqueous solution of **1** in the presence of one equivalent of pyrene increases the size in *ca*. 50 % while in the case of more water soluble hosts, **2** and **3**, a decrease on the size (*ca*. 15 and 40 %) is evidenced by this technique (see Figure S19). That means that host:guest interactions not only affects the aggregates' formation but also the intermolecular supramolecular arrangement.

Since the fluorescence spectrum of pyrene is sensitive to changes on its microenvironment, this technique is useful in probing the encapsulation and interaction of aromatic molecules within the inner cavities of the tripodal complexes.[48] This is detected by changes on the relative intensity between the first and the third pyrene emission peaks (I_1/I_3) which is known to be sensitive to the polarity of the microenvironment where it is placed.[49] The reasons for these observations have been attributed to excited state interaction of the molecule with the surrounding solvent and solvent reorientation around the excited state dipole.[50,51]

The I_1/I_3 ratio was found to vary with the concentration of the tripodal complexes in water (Figures 6 and S20-22). The decrease in I_1/I_3 in emission spectra at a higher concentration of gold complexes, indicates the partitioning of pyrene from an aqueous environment to a more hydrophobic location (Table 1 left). As expected, the recorded changes are slightly higher in the case of **1**, containing the most hydrophobic phosphine, PTA. The variations on the I_1/I_3 ratio in the presence of pyrene recorded in all cases are well fitted by a binding isotherm for 1:1 complexation and allowed the determination of the association constants for the formation of the adducts (Table 2).

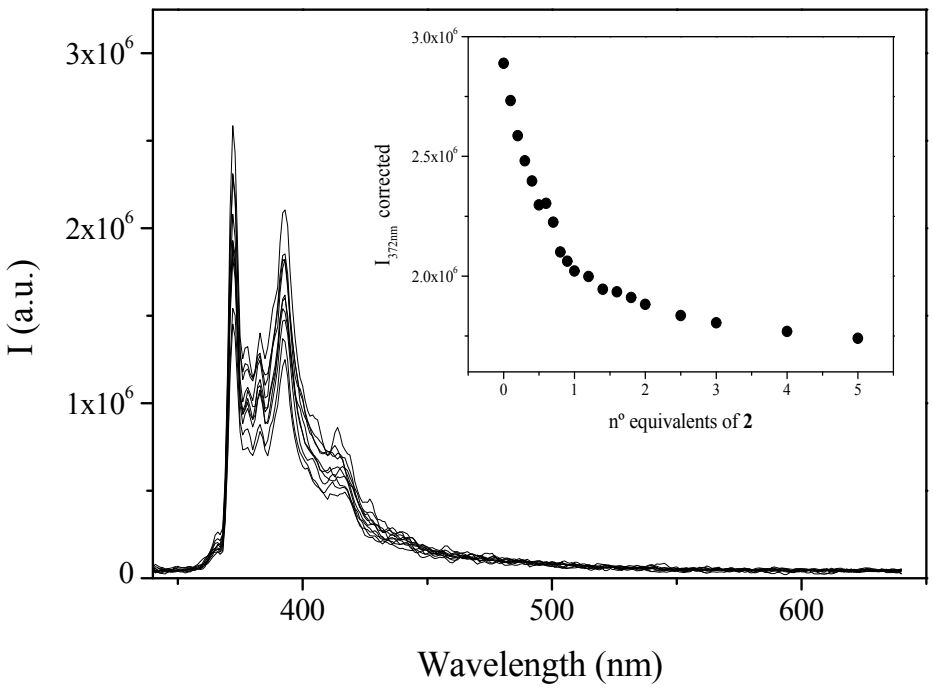

View Article Online
DOI: 10.1039/C9NJ00469F

Figure 6. Emission spectra of a $1 \cdot 10^{-5}$M solution of pyrene in the presence of increasing amounts of **2**. Inset: plot of the variation of $I_{372\ nm}$ vs number of equivalents of host.

Table 1. Calculated I_1/I_3 ratio as indication of pyrene polarity environment.

Compound	I_1/I_3 ratio	Sample	I_1/I_3 ratio
pyrene	1.89	pyrene @ cholate	0.86
pyrene : **1**	1.65	pyrene : **1**@cholate	1.10
pyrene : **2**	1.72	pyrene : **2**@cholate	1.12
pyrene : **3**	1.71	pyrene : **3**@cholate	0.87

Table 2. K_{ass} values (log$K$) of the formation of adducts between gold(I) complexes (**1**-**3**) and pyrene. Estimated error: 4%

Compound	log$K$
1	5.3
2	5.8
3	5.1

As stated above, the occurrence of C-H···π and Au···H-C interactions can be related to the host:guest adduct formation, since this kind of contacts have been previously detected in the X-ray crystal structures of gold(I) alkynyl complexes with arenes.[28] This could be the main reason for the higher K_{ass} value retrieved for **2**, due to the possible

presence of additional C-H···π interactions between the acetyl moieties and pyrene. Additionally, the lack of significant quenching observed in the case of **1** let us affirm that Au···π, C-H···π or N-H···π adducts are not producing quenching while the oxygen electron pairs coming from phosphines in **2** and **3** may be directly related with this phenomena.

Theoretical Calculations

In an attempt to understand the structure of pyrene@adducts, we have performed theoretical study using DFT calculations with complex **1** as a model. The different molecular geometries have been optimized in order to evaluate their relative stabilities and to determinate the nature of pyrene···**1** interactions. These modelled geometries are shown in the Figure 7, namely by a capital letter.

The structure of the trinuclear gold complex provides a feasibility to incorporate a pyrene molecule within the cavity. In consequence, model **A** that contains pyrene between the planes of **1** results as the most stable structure. The molecular analysis of this geometry shows short C-H group of the phosphine ligand and aromatic carbon atoms having distances until 2.9 Å indicating the presence of C-H···π interactions. Nevertheless, pyrene can rotate 90º keeping molecular plane as **B**, and it is destabilized by only 0.75 kcal/mol, probably by increasing of phosphine···pyrene distances. In both **A** and **B** models, our study suggests that the ratio between pyrene and **1** would be 1:1.

View Article Online
DOI: 10.1039/C9NJ00469F

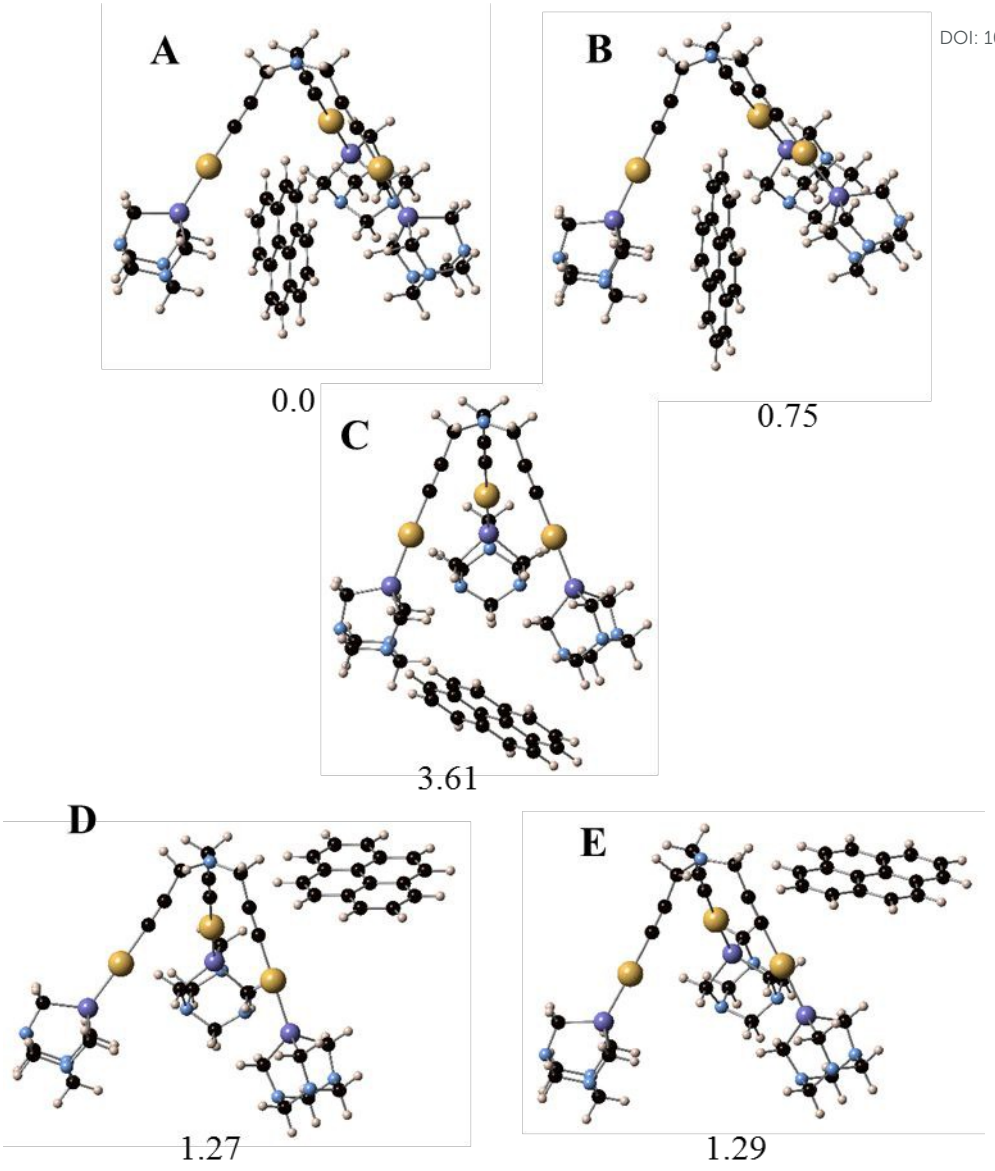

Figure 7. Full optimized structures for pyrene@**1** adducts, together with the relative stability. Energies are provided in kcal/mol, taken the most stable as reference (**A**).

On the other hand, we have considered the possibility to leave the pyrene outside of trinuclear gold compound. In this case, two models have been computed, **D** and **E**, having different rotation of pyrene to interact with trigold compound. The final geometries show interactions between C-H and C≡C groups of pyrene and alkynyl fragments, respectively, even that initial calculations were started to present C-H···Au contacts. In **D**, these non-bonded distances are about 2.9 and 3.5 Å, respectively, indicating that former is the driving force to generate the adduct. The relative stability

of **D** is only 1.27 kcal/mol above **A** and it could be accessible, but a second pyrene could be added on following face of trigold compound being in disagreement with 1:1 ratio. Analogously, **E** presents larger contacts that **D** resulting more unfavored. Moreover, our study also reveals that interactions between phosphine and pyrene of **C**, having largest C-H···π interactions, is less preferred of the five calculated models, and it can be rejected.

Stability in cholate gels

Gold···pyrene interactions were also analysed after the inclusion of the gold(I) complexes within cholate hydrogels (see Figure S23), synthesized following the literature method,[52] in order to get some additional information about the stability of this interaction in different environments. This matrix has been very well studied by Maitra's research group together with the effect of metal cations in the gelation process.[52] The high stability, bio-compatibility and lack of toxicity observed in these studies encouraged us to use it to include our systems and analyse if the stability of our supramolecular assemblies is also maintained in this thicker environment. For this goal, the formation of this organic/organometallic matrices was carried out by the introduction of: i) gold(I) complexes; ii) pyrene; and iii) both host and guest molecules in 1:1 ratio.

The presence of small aggregates (due to the presence of gold complexes) located on the cholate fibers are clearly observed in the case of **1** and **2** (Figure 8 B-C). A particular case was the inclusion of the negatively charged complex **3**. As can be seen in Figure 8D, this compound is directly taking part of the cholate matrix due to its ionic nature and no aggregates are deposited onto the cholate fibers.

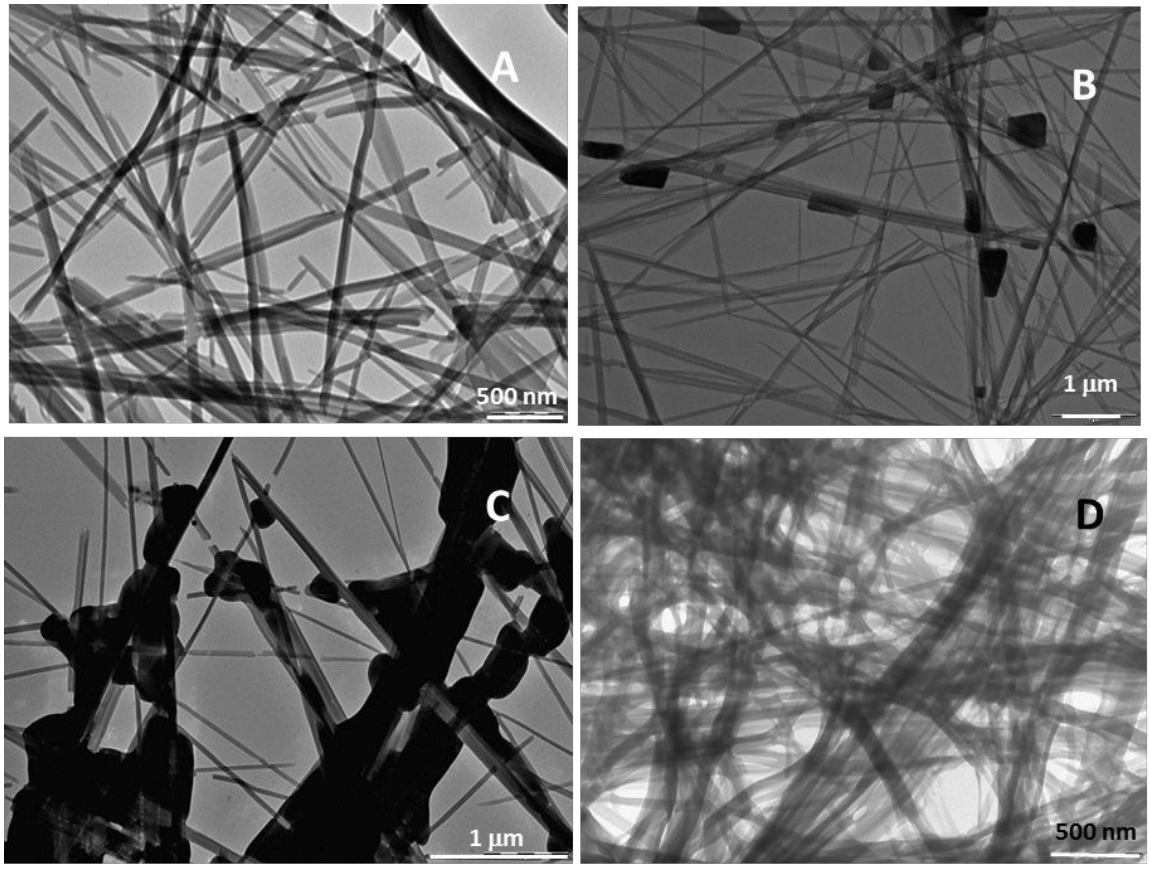

Figure 8. Transmission electron microscopy images of dried samples of cholate hydrogel (A); **1** @ cholate (B); **2** @ cholate (C) and **3** @ cholate (D).

Divalent cation cholate hydrogels are known to show liquid crystalline schlieren textures[52] when the wet gels are investigated in a polarizing optical microscope. As previously observed, the xerogels (dried gels) did not show any birefringence suggesting that the liquid crystalline behaviour in the wet hydrogels arise from the anisotropy created by the immobilized water inside the self-assembled nanofibres. These liquid crystalline properties of the metal cholate hydrogels show that they have a positional long-range order which is not always true for molecular gels as they might

have isotropic phases without any long-range order.[53] These properties are maintained in the presence of gold(I) complexes (Figure S24).

Analogous organic/organometallic hybrid systems were obtained in the presence of one equivalent of pyrene. The resulting optical and electronic microscopy images indicate the presence of both gold(I) complexes and pyrene within the cholate matrix. Inspection of Figure S25 shows the presence of larger and more brilliant aggregates in the case of **1** and **2** although it is not so clear with **3** in agreement with the presence of this complex within the cholate structure and not as agglomerates located on the fibers. Inspection of the samples by TEM shows the presence of white plates, assigned to pyrene deposition (Figure 9), located above the darker organometallic aggregates. It should be noted that these observations must be performed at very low electron beam irradiation since, as previously observed in other gold(I) alkynyl complexes, the formation of Au(0) nanoparticles is induced by electrons[54] (Figure S26).

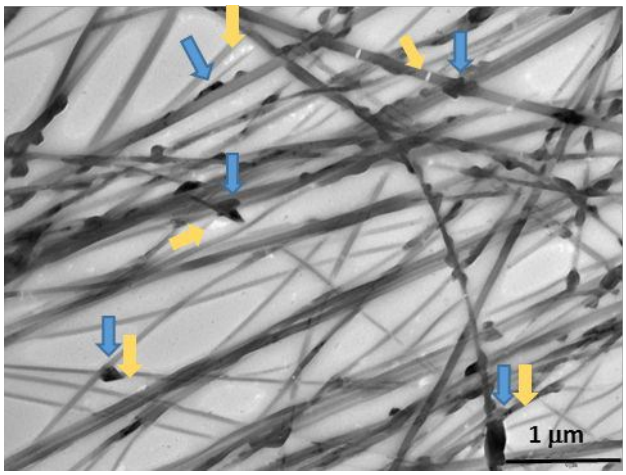

Figure 9. TEM image of **2** : pyrene @ cholate. White plates (orange arrows) are indicative of pyrene and black agglomerates (blue arrows) indicate **2**-supramolecular structures.

The recorded emission spectra of pyrene@cholate samples in the presence and in the absence of **1-3** are a direct evidence of pyrene:gold interaction in the case of the neutral complexes **1** and **2** as it is displayed by the changes on the I_1/I_3 ratio (Figure 10 and Table 1 right) which seem to be slightly favoured in the presence of **1** due to its higher hydrophobic character.

View Article Online
DOI: 10.1039/C9NJ00469F

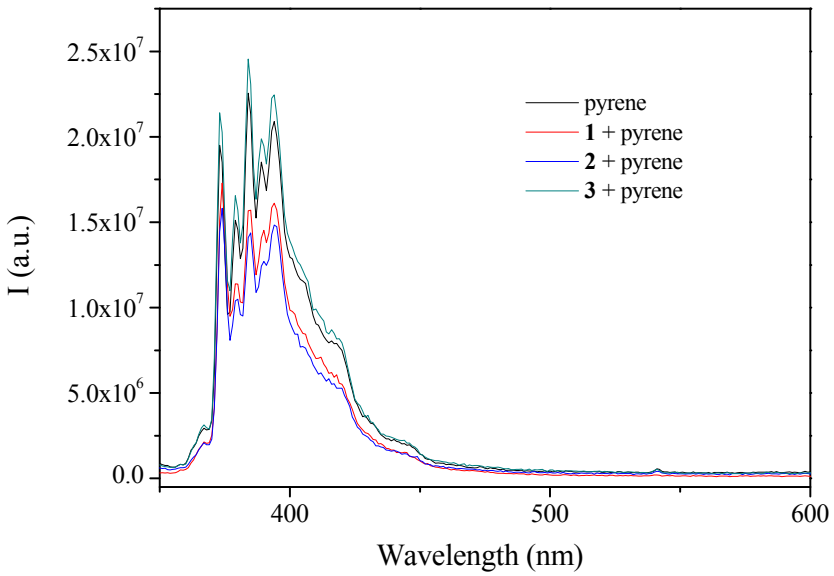

Figure 10. Emission spectra of pyrene@cholate, pyrene : **1**@cholate, pyrene : **2**@cholate and pyrene : **3**@cholate.

The lack of effect observed for pyrene : **3**@cholate is due to the ionic nature of this complex included within the organic matrix precluding the interaction with the arene. Additionally, and on the basis of literature data,[55] changes in signal intensity or shifts in the maxima of the spectrum could indicate complex formation. The decrease on the recorded intensity of pyrene in the presence of **1** and **2** is a further indication of the successful **1** / **2**-pyrene adduct formation within the organic matrix.

Thus, tripodal gold(I) complexes have been demonstrated to be good candidates to act as supramolecular hosts of organic molecules in water taking into consideration the hydrophobic character of both gold(I) atoms and organic counterpart. These interactions can be reinforced by the possible establishment of Au···π interactions additionally to classical weak contacts and they are stable with their introduction into cholate organic matrixes as solid supports in the case of neutral complexes that do not compete with the matrix hydrogelation process.

Conclusions

The formation of large supramolecular assemblies in gold(I) tripodal derivatives is favoured by concentration and time. The resulting aggregates' formation depends on the solubility in water of the phosphine being an enthalpic (for **2** and **3**) or entropic (in the case of **1**) driving process. Entropic factors are ascribed to the release of water molecules upon aggregation (hydrophobic effect) in complex **1**. This behaviour is also observed with the complex containing the highly water soluble and negatively charged trisulphonated phosphine TPPTS, although longer times are required.

^{1}H NMR spectroscopy together with SAXS and microscopic techniques (OM and TEM) give information about the formation of the aggregates and their sizes. SAXS and microscopic techniques are important for the analysis of their shape.

The presence of hydrophilic groups (phosphines) and hydrophobic moieties (organic part and gold centers) within the same molecules make these complexes ideal candidates to interact with aromatic molecules within the supramolecular structure as has been demonstrated in the case of pyrene. DFT studies suports the formation of gold:pyrene adducts with the most stable expected conformation with the aromatic moiety within the tripodal cavity.

The interaction with pyrene is produced both in water and in cholate gelators being stable in both cases for neutral derivatives while the presence of negative charges in the TPPTS phosphine in **3** makes the compound to become an integral part of the cholate fibrillar network. Additionally, the higher solubility in water of DAPTA (**2**) compared to PTA (**1**) gives rise to stronger adduct formation with pyrene.

Experimental Section

General procedures. All manipulations have been performed under prepurified N_2 atmosphere using Schlenk techniques. All solvents were distilled from appropriated drying agents. MilliQ water quality was used for the preparation of the corresponding solutions. The pH of the solutions was maintained neutral in order to ensure the neutral state of the amine groups. Deuterated solvents were obtained from Aldrich and were used as received except chloroform that was treated with alumina and under nitrogen atmosphere. Commercial reagents 1,3,5-triaza-7-phosphaadamantane (PTA, Aldrich, 97%), 3,7-diacetyl-1,3,7-triaza-5-phosphabicyclo[3.3.1]nonane (DAPTA, Aldrich, 97%), triphenylphosfine-3,3',3''-trisulfonic acid trisodium salt (TPPTS, Aldrich, ≥95%) have been used as received, Literature methods were used to prepare [AuCl(PR'$_3$)] (PR'$_3$ = PTA,[56] DAPTA.[56]

Physical Measurements. IR spectra were recorded as KBr disk with IR-Avatar 330 *FT*-IR Thermo Nicolet. ^{1}H NMR (δ(TMS)=0.00) and ^{31}P{^{1}H} NMR spectra were recorded with a Varian Mercury 400 and Bruker 400. ^{1}H NMR studies at different concentrations performed to evaluate aggregation process have been performed using long relaxation delays of 5-10 times T1 and the differences of integration with concentration have been strickly evaluation with respect to TSP used as reference. ElectroSpray-Mass Spectra (+/-) were measured with a Fision VG Quatro spectrophotometer. The water used for the solutions of absorption and emission measurements was obtained through a Milliport Ven Filter MPK01. Absorption spectra were recorded with UV-visible Varian Cary 100 Bio spectrophotometer. Emission spectra were recorded with Nanolog-Horiba Jobin Yvon spectrofluorimeter. Optical micrographs were recorded with a Leica DM1000LED and TEM images were recorded with a Tecnai G2 Spirit microscope. The measurements were acquired using a carbon TEM support films on cooper where the cholate hydrogels were deposited the day before and dried during 24h.

Small angle X-ray scattering

SAXS data have been performed on the NCD-SWEET beamline at the synchrotron ALBA at 12.4 keV and the distance sample/detector was 6.2m to cover the range of momentum transfer $0.028 < q < 2.56$ nm^{-1}. The data were collected on a Pilatus3S 1M detector with a pixel size of 172.0x172.0μm^2. The exposure time was 30s. The q-axis

calibration was obtained by measuring silver behenate.[57] The program pyFAI[58] was used to integrate the 2D SAXS data into 1D data.

The data were then subtracted by the background using *PRIMUS* software.[59] The maximum particle dimension D_{max} and the pair-distance distribution function $P(r)$ were determined with *GNOM*.[60] The low-resolution structure of the aggregates was reconstructed ab initio from the initial portions of the scattering patterns using the program DAMMIN.[39]

$1 \cdot 10^{-4}$ M and $1 \cdot 10^{-5}$M solutions of complexes **1-3** were prepared in different water/DMSO mixtures (0, 25, 50, 75, 90% water contents) and also for gold complex: pyrene solutions (1:1) at $1 \cdot 10^{-5}$M concentration of host.

Spectroscopic absorption and emission titrations

A 0.1mL aliquot of a $1 \cdot 10^{-3}$ M solution of pyrene in CH_2Cl_2 was added to a 10 mL volumetric flask. The solvent was evaporated and MilliQ water was added to the mark. The flask was sonicated for 10 min before use. HCl 0.1M and NaOH 0.1M were used to adjust the pH values to 7, which were measured on a MeterLab 240 pH meter.

Absorption titrations. 3 ml of a neutral $1 \cdot 10^{-5}$M aqueous solutions of pyrene were introduced in a 1 cm path absorption cuvette. Different amounts of neutral aqueous gold(I) complex (**1-3**) solutions were introduced both in the sample cuvette and at the blank cuvette in order to perform differential absorption spectroscopy and record the resulting spectra of the pyrene:gold adduct.

Emission titrations. 3 ml of a $1 \cdot 10^{-5}$M aqueous solutions of pyrene were introduced in a 1 cm path emission cuvette. Different amounts of neutral aqueous gold(I) complex (**1-3**) solutions were introduced in the cuvette and the corresponding emission spectra were recorded in each point. The resulting variations recorded for the emission were plot against number of equivalents of gold complex added. The resulting data was fitted following the equation derived by Lehn[61] in order to retrieve the association constants values.

Theoretical Calculations.

Calculations were carried out using the Gaussian09 package.[62] The hybrid density function method known as B3LYP was applied.[63,64] All electron basis sets having

valence triple-ζ quality adding a polarization function in all atoms were used.[65,66] Geometry optimizations were carried out on the full potential-energy surface without symmetry restrictions and confirmed as mínima by vibrational analysis.

Preparation of cholate hydrogels

The preparation of these hydrogels has been performed following the procedure reported in the literature.[52,67] In case of doped hydrogels containing gold complexes and pyrene, the gelation has been carried out adding 50 μL of the $1 \cdot 10^{-4}$M solutions of **1-3** on a 1.5 mL of 30 mM solution of $Zn(NO_3)_2 \cdot 6H_2O$. Then, 1.5 mL of a solution of sodium cholate (60 mM) is added at room temperature. The sonication (ultrasonic bath) during 25-30 seconds facilitates the gel formation.

A solution of pyrene (9 μL, $5.5 \cdot 10^{-4}$M) was also added in the formation of the cholate hydrogels containing this chromophore.

Synthesis and Characterization

Synthesis of AuCl(TPPTS).

This complex was synthesized following a slight modification of the previously reported procedure.[9] A solution of triphenylphosfine-3,3',3''-trisulfonic acid trisodium salt, TPPTS, (0.1500 g, 0.264mmol) in methanol (15 mL) was added to a solution of [AuCl(tht)] (0.1029g, 0.264 mmol) in dichloromethane (15 mL). After 24 hour of stirring the solution was concentrated to *ca.* 15 mL and diethyl ether (20 mL) was added in order to initiate the precipitation of a white product. The solid was separated by filtration, recrystallized with dichloromethane /diethyl ether and dried under vacuum. Yield: 45% (0.0691 g). IR (KBr, cm^{-1}): 3055 (C_{sp^2}-H), 1465 (C=C), 1280 and 1034 (S=O).^{1}H NMR (D_2O, 400 MHz): δ 8.15-8.00 (m,6H, P-C-C*H*-C-S + S-C*H*-CH), 7.85-7.65 (m, 6H, CH-C*H*-CH + P-C-C*H*-CH) ppm. ^{31}P NMR (D_2O, 162.0 Hz): δ 34.1 ppm.

Synthesis of $N[Au(C\equiv C\text{-}CH_2)PTA]_3$ (1)

This compound was prepared following a slightly modified previously described methodology.[36] KOH (0.038g, 0.67 mmol) was added to a solution of tripropargylamine (30 μL, 0.21 mmol) in methanol (15 mL). After 30 min stirring, was added a solution of

[AuClPTA] (0.252g, 0.646 mmol) in dichloromethane (25 mL). After 96 hours of stirring the solution was filtered through Celite, concentrated to *ca.* 20 mL and hexane (20 mL) was added in order to initiate the precipitation of an orange solid. The product was isolated by filtration, and then recrystallized with dichloromethane/ hexane and dried under vacuum. Yield: 52% (0.133g). IR (KBr, cm^{-1}): 1240 (C-N), 2000 (C≡C), 728 (C-P). ^1H NMR ($CDCl_3$:, 400 MHz): δ 4.57 (d, J=12.8 Hz, 9H, N-CH_2-N), 4.49 (d, J=12.8 Hz, 9H, N-CH_2-N), 4.30 (s, 18H, N-CH_2-P), 3.5 (s, 6H, C-CH_2-N) ppm. ^{31}P NMR ($CDCl_3$, 161.9 MHz): δ -40.1 ppm. ESI-MS(+): m/z 1191.1977 ($[M + H]^+$; calcd m/z 1191.1903). Anal. Calcd (%) for $C_{27}H_{42}Au_3N_{10}P_3$: C 27.24, H 3.56, N 11.77. Found: C 27.57, H 3.30, N 12.00.

Synthesis of N[Au(C≡C-CH_2)DAPTA]$_3$ (2)

This compound was prepared following a slightly modified previously described methodology.[38] The same procedure than in the synthesis of **1** was used but stirring the reaction mixture for 72 h instead of 96 h and using AuCl(DAPTA) (0.243 mg, 0.528 mmol) instead of AuCl(PTA) and 26 µL (0.183 mmol) of tripropargylamine and 0.038 g (0.67 mmol) of KOH. Yield: 35% (0.087 g). IR (KBr, cm^{-1}): 2098 (C≡C), 1630 (C=O), 1427 (CH_2-P), 1234 (C-N). ^1H NMR ($CDCl_3$, 400 MHz): δ 5.82-5.63 (m, 6H, N-CH_2-N + N-CH_2-P), 4.85-4.95 (m, 3H, N-CH_2-N), 4.70-4.65 (m, 6H, N-CH_2-P + N-CH_2-N), 4.10-4.06 (m, 6H, N-CH_2-P + N-CH_2-N), 3.85 (s, 6H, N-CH_2-P), 3.55 (s, 3H, N-CH_2-P), 3.50 (s, 6H, C-CH_2-N), 2.11 (s, 18H, CO-CH_3) ppm. ^{31}P NMR (D_2O, 161.9 MHz): δ -13.9 ppm. ESI-MS(+): m/z 1407.2604 ($[M + H]^+$; calcd m/z 1407.2603). Anal. Calcd (%) for $C_{36}H_{54}Au_3N_{10}O_6P_3$: C 30.74, H 3.87, N 9.96. Found: C 30.65, H 3.82, N 10.12.

Synthesis of N[Au(C≡C-CH_2)TPPTS]$_3$ (3)

The synthesis of this compound was performed following the same experimental procedure than in **2** but using only methanol as solvent and diethyl ether as precipitating agent instead of hexane and AuCl(TPTTS) (0.250 mg, 0.312 mmol) instead of AuCl(PTA) and 15 µL (0.106 mmol) of tripropargylamine and 0.018 g (0.315 mmol) of KOH.Yield: 16% (0.040 g). White solid. IR (KBr, cm^{-1}): 3055 (C_{sp^2} – H), 2100 (C≡C), 1465 (C=C (Ar)), 1034 (S=O). ^1H NMR (D_2O, 400MHz): δ 8.06-7.35 (m, 36H, Ph_o +

Ph_m + Ph_p), 3.60-3.50 (s, 6H, N-CH_2-C≡C) ppm. ^{31}P NMR (D_2O, 161.9 MHz): δ 42.5 ppm. ESI-MS(-): m/z 773.2966 ([M- $7Na^+$+$4H^+$+$3H_2O$]$^{3-}$; calcd m/z 773.2988). Anal. Calcd (%) for $C_{63}H_{42}Au_3NNa_9O_{27}P_3S_9$: C, 31.21; H, 1.75; N, 0.58; S, 11.90. Found: C, 30.97; H, 1.74; N, 0.62; S, 12.03.

Acknowledgements

The authors are grateful to the Ministry of Economy, Industry and Competitiveness of Spain (AEI/FEDER, UE Project CTQ2016-76120-P). This work was also supported by the Associated Laboratory for Sustainable Chemistry, Clean Processes and Technologies, LAQV, which is financed by national funds from FCT/MEC (UID/QUI/50006/2013) and co-financed by the ERDF under the PT2020 Partnership Agreement (POCI-01-0145-FEDER-007265). This research was supported by a Marie Curie Intra European Fellowship within the 7th European Community Framework Programme (R.G.). A.M. thanks FCT for a post-doctoral grant (SFRH/BPD/69210/2010). SAXS experiments were performed at the NCD-SWEET beamline of the ALBA Synchrotron Light Facility in collaboration with the ALBA staff. Allocation of computer facilities at IQTCUB is also acknowledged, supported by María de Maeztu program (MDM-2017-0767).

Supporting Information

^{1}H and ^{31}P{^{1}H} NMR characterization data of **1-3**. ^{1}H NMR spectra at different concentrations; SAXS data of **1-3** at different concentrations and temperatures; Optical microscoy images of **1-3** at $1 \cdot 10^{-4}$M; absorption and emission titrations of pyrene in the presence of **1-3**. Optical and electronic microscopy images of hybrid cholate aggregates.

References

[1] B. H. Northrop, Y.-R. Zheng, K.-W. Chi and P. J. Stang, *Acc. Chem. Res*., 2009, **42**, 1554.

[2] L. A. Estroff and A. D. Hamilton, *Chem. Rev*., 2004, **104**, 1201;

[3] A. Pinto, N. Svahn, J.C. Lima and L. Rodríguez, *Dalton Trans.* 2017, **46**, 11125.

[4] a) R. E. Bachman, A. J. Zucchero and J. L. Robinson, *Langmuir*, 2012, **28**, 27; (b) P. Terech, G. Gebel and R. Ramasseul, *Langmuir*, 1996, **12**, 4321; (c) B. Xing, M. F. Choi, Z. Zhou and B. Xu, *Langmuir*, 2002, **18**, 9654.

[5] J.C. Lima and L. Rodríguez, *Inorganics* 2015, **3**, 1.

[6] P. Howlader and P. S. Mukherjee, *Chem. Sci*., 2016, **7**, 5893.

[7] Y.-X. Ye, W.-L. Liu and B.-H. Ye, *Catal. Commun.* 2017, **89**, 100.

[8] M. Araújo and B. Escuder, *ChemistrySelect* 2017, **2**, 854.

[9] S. Sanz, L.A. Jones, F. Mohr, M. Laguna. *Organometallics* 2007, **26***,* 952.

[10] P. Sutar and T. K. Maji, *Chem.Commun*., 2016, **52**, 8055.

[11] L. Giestas, R. Gavara, E. Aguiló, N. Svahn, J.C. Lima and L. Rodríguez, *Supramol. Chem.*, 2018, **30**, 278.

[12] E. Aguiló, A.J. Moro, R. Gavara, I. Alfonso, Y. Pérez, F. Zaccaria, C. Fonseca Guerra, M. Malfois, C. Baucells, M. Ferrer, J.C. Lima and L. Rodríguez, *Inorg. Chem.* 2018, **57**, 1017.

[13] A. Kishimura, T. Yamashita and T. Aida, *J. Am. Chem. Soc*., 2005, **127**, 179.

[14] B. D. Yuhas, A. L. Smeigh, A. P. S. Samuel, Y. Shim, S. Bag, A. P. Douvalis, M. R. Wasielewski and M. G. Kanatzidis, *J. Am. Chem. Soc*., 2011, **133**, 7252.

[15] X. He, Y. Xue, C.-C. Li, Y. Wang, H. Jiang and L. Zhao, *Chem. Sci.*, 2018, **9**, 1481.

[16] L. Fü, Y. Fang and G.J. Blanchard *Spectrochim Acta A Mol Biomol. Spectrosc* 2009, **74**, 991.

[17] R. Ferrer, J.L. Beltrán and J. Guiteras, *Talanta* 1998, **45**, 1073.

[18] N. P.E. Barry, O. Zava, W. Wu, J. Zhao and B. Therrien, *Inorg. Chem. Commun*. 2012, **18**, 25.

[19] A. M. Lifschitz, M. S. Rosen, C. M. McGuirk and C. A. Mirkin, *J. Am. Chem. Soc*., 2015, **137**, 7252.

[20] B. Kemper, Y.R. Hristova, S. Tacke, L. Stegemann, L.S. van Bezouwen, M.C.A. Stuart, J. Klingauf, C.A. Strassert and P. Besenius, *Chem. Commun*. 2015, **51**, 5253.

[21] E. Lee, H. Ju, Y. Kang, S. S. Lee, K.-M. Park, *Chem. Eur. J.* 2015, **21**, 6052.

[22] O. Abdel-Aziz, A. M. El Kosasy and S. M. El-Sayed Okeil, *J Fluoresc* 2014, 24, 549.

[23] V.N.S. Occello and A.V. Veglia, *Anal. Chim. Acta* 2011, **689**, 97.

[24] M. Kfoury, D. Landy and S. Fourmentin, *Molecules* 2018, **23**, 1204.

[25] R. R. Kashapov, S.V. Kharlamov, E.D. Sultanova, R.K. Mukhitova, Y.R. Kudryashova, L.Y. Zakharova, A.Y. Ziganshina and A.I. Konovalov, *Chem. Eur. J.* 2014, **20**, 14018.

[26] R. Gramage-Doria, D. Armspach, D. Matt, *Coord. Chem. Rev*. 2013, **257**, 776.

[27] L. Rodríguez, J.C. Lima, M. Ferrer, O. Rossell, M. Engeser, *Inorg. Chim. Acta* 2012, **381**, 195.

[28] V. Mishra, A. Raghuvanshi, A. Kumar Saini and S. M. Mobin, *J. Organomet. Chem*. 2016, **813**, 103.

[29] N. Svahn, A.J. Moro, C. Roma-Rodrigues, R. Puttreddy, K.Rissanen, P.V. Baptista, A. R. Fernandes, J.C. Lima and L. Rodríguez, *Chem.-Eur. J.* 2018, **24**, 14654.

[30] X. He, E. C.-C. Cheng, N. Zhu, V. W.-W. Yam, *Chem. Commun.*, 2009, 4016.

[31] Y.-P. Zhou, E.-B. Liu, J. Wang, H.-. Chao, Inorg. Chem. 2013, 52, 8629.

[32] J.F. Fernández-Sánchez, A. Segura Carretero, C. Cruces-Blanco and A. Fernández-Gutiérrez, *Anal. Chim. Acta* 2011, **506**, 1.

[33] D. Patra and A.K. Mishra, *Talanta* 2001, **55**, 143.

[34] G. Bains, A. B. Patel and V. Narayanaswami, *Molecules* 2011, **16**, 7909.

[35] S. V. Aathimanikandan, E. N. Savariar and S. Thayumanavan, *J. Am. Chem. Soc.* 2005, **127**, 14922.

[36] R. Laishram and U. Maitra, *Chem. Asian J.* 2017, **12**, 1267.

[37] A. Chakrabarty, U. Maitra and A. D. Das, *J. Mater. Chem.* 2012, **22**, 18268.

[38] E. Vergara, E. Cerrada, A. Casini, O. Zava, Mariano Laguna and P. J. Dyson, *Organometallics* 2010, **29**, 2596.

[39] (a) D. I. Svergun, Restoring Low Resolution Structure of Biological Macromolecules from Solution Scattering Using Simulated Annealing. *Biophys J.*, 1999, 2879. (b) A. Krebs, H. Durchschlag and P. Zipper, Small Angle X-Ray Scattering Studies and Modeling of Eudistylia vancouverii Chlorocruorin and Macrobdella decora Hemoglobin. *Biophys J.*, 2004, **2**, 1173.

[40] T. I. Mizan, P. E. Savage and R. M. Ziff, *J. Phys. Chem.* 1996, **100**, 403.

[41] R. Gavara, E. Aguiló, C. Fonseca Guerra, L. Rodríguez and J.C. Lima, *Inorg. Chem.* 2015, **54**, 5195.

[42] S. Pandey, M. Ali, A. Bishnoi, A. Azam, S. Pandey and H.M. Chawla, *J. Fluoresc*. 2008, **18**, 533.

[43] D. Kim, R. Amos, M. Gauthier and J. Duhamel, *Langmuir* 2018, **34**, 8611.

[44] A. Yekta, J. Duhamel, P. Brochard, H. Adiwidjaja and M.A. Winnik, *Macromolecules* 1993, **26**, 1829.

[45] E. R. T. Tiekink and J. Zukerman-Schpector, *Cryst. Eng. Comm*, 2009, **11**, 1176.

[46] D. Nolan, B. Gil, L. Wang, J. Zhao and S.M. Draper, *Chem. Eur. J.* 2013, **19**, 15615.

[47] L. Rodríguez, J.C. Lima, M. Ferrer, O. Rossell and M. Engeser, *Inorg. Chim. Acta* 2012, **381**, 195.

[48] V. Ramamurthy, S. Jockusch and M. Porel, *Langmuir* 2015, **31**, 5554.

[49] D. C. Dong and M. A. Winnik *Can. J. Chem*. 1984, **62**, 2560.

[50] J.R. Lakowicz, Solvent effects on emission spectra. In *Principles of Fluorescence Spectroscopy*, 2nd ed.; Lakowicz, J.R., Ed.; Kluwer Academic/ Plenum Publisher: New York, NY, USA, 1999; pp. 185-189.

[51] A. Nakajima, *J. Mol. Spectrosc.* 1976, **61**, 467.

[52] A. Chakrabarty, U. Maitra and A.D. Das, *J. Mater. Chem.* 2012, **22**, 18268.

[53] Molecular Gels, Materials with Self-Assembled Fibrillar Networks, ed. R. G. Weiss and P. Terech, Springer, 2006, pp. 751–752.

[54] E. Aguiló, R. Gavara, J.C. Lima, J. Llorca and L. Rodríguez, *J. Mater. Chem. C* 2013, **1**, 5538.

[55] K.A. Connors, Binding Constants: The Measurement of Molecular Complex Stability, John Wiley & Sons, New York, 1987.

[56] E. Vegara, S. Miranda, F. Moh, E. Cerrada, E.R.T. Tiekink, P. Romero, A. Mendía and M. Laguna. *Eur. J. Inorg. Chem.*, 2007, 2926.

[57] T. C. Huang, H. Toraya, T. N. Blanton and Y. Wu, *J. Appl. Cryst*., 1993, **26**, 180.

[58] J. Kieffer and D. Karkoulis, *J. Phys.: Conf. Ser.*, 2013, **425**, 202012.

[59] J. App, V. Konarev, V. V. Volkov, A. V. Sokolova, M. H. J. Koch and D. I. Svergun, *J. Appl. Cryst*., 2003, **36**, 1277.

[60] D. I. Svergun, *J. Appl Cryst.*, 1992, **25**, 495.

[61] P. Cjudić, M. Zjinić, V. Tomisjić, V. Simeon, J.-P. Vigneron and J.-M. Lehn, *J. Chem. Soc., Chem. Commun.* 1995, 1073.

[62] M. J. Frisch, G. W. Trucks, H. B. Schlegel, G. E. Scuseria, M. A. Robb, J. R. Cheeseman, G. Scalmani, V. Barone, B. Mennucci, G. A. Petersson, H. Nakatsuji, M. Caricato, X. Li, H. P. Hratchian, A. F. Izmaylov, J. Bloino, G. Zheng, J. L. Sonnenberg, M. Hada, M. Ehara, K. Toyota, R. Fukuda, J. Hasegawa, M. Ishida, T. Nakajima, Y. Honda, O. Kitao, H. Nakai, T. Vreven, J. A. Montgomery, Jr., J. E. Peralta, F. Ogliaro, M. Bearpark, J. J. Heyd, E. Brothers, K. N. Kudin, V. N. Staroverov, T. Keith, R. Kobayashi, J. Normand, K. Raghavachari, A. Rendell, J. C. Burant, S. S. Iyengar, J. Tomasi, M. Cossi, N. Rega, J. M. Millam, M. Klene, J. E. Knox, J. B. Cross, V. Bakken, C. Adamo, J. Jaramillo, R. Gomperts, R. E. Stratmann, O. Yazyev, A. J. Austin, R. Cammi, C. Pomelli, J. W. Ochterski, R. L. Martin, K. Morokuma, V. G. Zakrzewski, G. A. Voth, P. Salvador, J. J. Dannenberg, S. Dapprich, A. D. Daniels, O. Farkas, J. B. Foresman, J. V. Ortiz, J. Cioslowski, D. J. Fox, Gaussian 09 (Revission B.1), Gaussian Inc., Wallingford CT, 2010.

[63] A. D. Becke, *J. Chem. Phys*. 1993, **98**, 5648.

[64] C. Lee, W. Yang R. G. Parr, *Phys. Rev. B* 1988, **37**, 785.

[65] A. Schaefer, C. Huber, R. Ahlrichs, *J. Chem. Phys*. 1994, **100**, 5829.

[66] D. Andrae, U. Haeussermann, M. Dolg, H. Stoll, H. Preuss, *Theor. Chim. Acta* 1990, **77**, 123

[67] R. Gavara, J. Mateos, F. Sabaté, R. Belda, J. M. Llinares, E. García-España and L. Rodríguez, *Eur. J. Inorg. Chem.* 2018, 4550.

View Article Online
DOI: 10.1039/C9NJ00469F

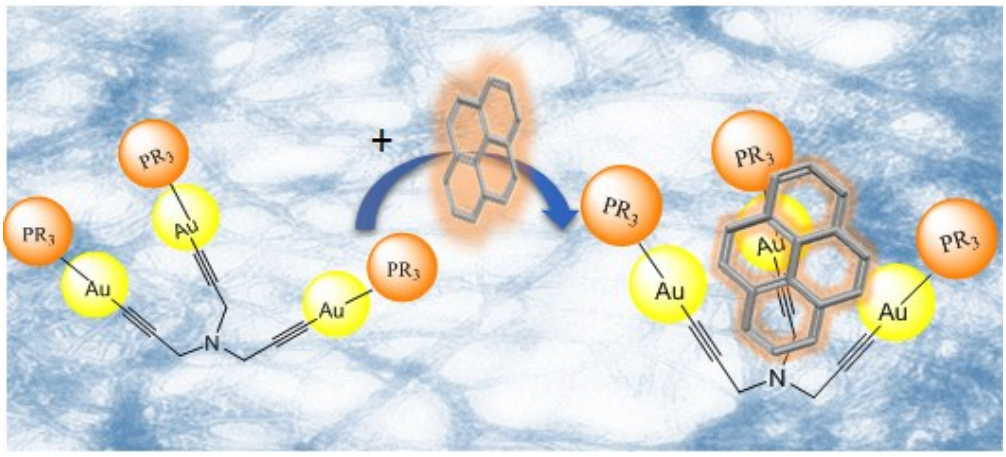

139x62mm (96 x 96 DPI)